Journal of Power Sources 220 (2012) 84–88

Contents lists available at SciVerse ScienceDirect

Journal of Power Sources

journal homepage: www.elsevier.com/locate/jpowsour

Short communication

Facile synthesis of nanocrystalline $Li_4Ti_5O_{12}$ by microemulsion and its application as anode material for Li-ion batteries

Guang-Yin Liu [a], Hui-Yuan Wang [a,*], Guo-Qiang Liu [b], Zhi-Zheng Yang [a], Bo Jin [a], Qi-Chuan Jiang [a,*]

[a] Key Laboratory of Automobile Materials of Ministry of Education, School of Materials Science and Engineering, Jilin University, No. 5988 Renmin Street, Changchun, Jilin Province 130025, China
[b] School of Materials and Metallurgy, Northeastern University, Shenyang 110819, China

HIGHLIGHTS

- The $Li_4Ti_5O_{12}$ is synthesized through a facile microemulsion route.
- As-prepared $Li_4Ti_5O_{12}$ features small size and high crystallinity.
- This nanocrystalline $Li_4Ti_5O_{12}$ exhibits superior electrochemical performance.

ARTICLE INFO

Article history:
Received 18 May 2012
Received in revised form
25 July 2012
Accepted 30 July 2012
Available online 7 August 2012

Keywords:
Li-ion batteries
Lithium titanate
Microemulsion
Nanocrystalline
Anode materials

ABSTRACT

Here, we report a facile approach for synthesizing nanocrystalline $Li_4Ti_5O_{12}$ by microemulsion at ambient temperature following by annealing treatment at 600 °C for 2 h for the first time. The X-ray diffraction, field emission scanning electron microscopy, transmission electron microscopy and nitrogen adsorption/desorption measurements are performed to characterize the structures and morphology of as-prepared sample. The as-prepared $Li_4Ti_5O_{12}$ nanocrystalline around 30–50 nm in size and has high crystallinity, which displays excellent discharge/charge rate capability and cycling stability as anode materials for Li-ion batteries. More importantly, specific capacities for $Li_4Ti_5O_{12}$ nanocrystalline achieved here are 173.7, 166.2, 136.2 and 130.2 $mAhg^{-1}$ at 0.2, 1, 5 and 10 C after 50 cycles, respectively, indicating high potential application for Li-ion batteries.

1. Introduction

Rechargeable Li-ion batteries (LIBs) have attracted great attention for their widespread applications in various portable electronics and electric vehicles (EVs) [1–3]. One of the key safety issues in LIBs for EVs, however, is the dendritic lithium growth on the conventional graphite anode surface at high charging current, owing to the relatively low Li^+ insertion potential of carbonous materials [4–7]. Moreover, Li-ion battery technology needs to be improved to generate more power, enjoy longer life cycle and less production cost [4,5]. Consequently, much attention has been focused on the development of new anode materials recently.

Spinel lithium titanate ($Li_4Ti_5O_{12}$) is regarded as a superior anode material for energy storage cells for its excellent insertion and extraction reversibility, safety and stable structure in charge–discharge process [8–10]. Despite many advantages associated with $Li_4Ti_5O_{12}$, low electric conductivity prohibits its large-scale applications due to its poor charge–discharge properties at high current rates [11,12]. Therefore, many methods have been attempted to improve the electric conductivity of $Li_4Ti_5O_{12}$, including doping with ions, coating with a conductive phase such as amorphous carbon and Ag, synthesizing nanosized materials to shorten path lengths for Li^+ transport, and fabricating a porous structure to absorb the electrolyte [13–17]. In particular, nano-structured $Li_4Ti_5O_{12}$ with various morphologies were successfully prepared and exhibited excellent rate capability and cycling stability [13,14,18–23]. Nano-sized $Li_4Ti_5O_{12}$ is generally synthesized by wet processes, such as sol–gel method [24], solution-combustion method [25] and hydrothermal method [13,14,21–23], etc.

* Corresponding authors. Tel./fax: +86 431 8509 4699.
E-mail addresses: wanghuiyuan@jlu.edu.cn (H.-Y. Wang), jiangqc@jlu.edu.cn (Q.-C. Jiang).

0378-7753/$ – see front matter © 2012 Elsevier B.V. All rights reserved.
http://dx.doi.org/10.1016/j.jpowsour.2012.07.087

Since the term "microemulsion" was introduced by Schulman, Stoeckenius and Prince for the first time in the late 1950s [26], microemulsion process (reverse micelle synthesis) has been developed to be a powerful approach to control particle size and size distribution, and widely used to synthesize various nanoscale crystallines, such as metallic, metal oxide, semiconductor (quantum dots) nanoparticles, and even more complex ceramic nanomaterials [27–30]. In this study, we first report a facile strategy to prepare nanocrystalline $Li_4Ti_5O_{12}$ by a simple microemulsion route followed by calcination at 600 °C for 2 h. The as-prepared nanocrystalline $Li_4Ti_5O_{12}$ was measured as an anode material for lithium ion battery, exhibiting high reversible capacity and good cycling performance even at high current densities.

2. Experimental procedure

2.1. Preparation of the $Li_4Ti_5O_{12}$

Analytical-grade $Ti(OC_3H_7)_4$, $LiOH\cdot H_2O$, *n*-pentanol, cyclohexane and cetyltrimethylammonium bromide (CTAB) were used as received without further purification. In a typical procedure to synthesize nanocrystalline $Li_4Ti_5O_{12}$, two microemulsion solutions were prepared by adding 2.5 mL of 10 mmol $Ti(OC_3H_7)_4$ and 2.5 mL of 8 mmol $LiOH\cdot H_2O$ aqueous solutions to *n*-pentanol/CTAB/cyclohexane mixtures in which the mol ratio of *n*-pentanol/CTAB was 4 and the concentration of CTAB aqueous solutions was 0.3 M, and was magnetically stirred for 10 min until it became a homogeneous and transparent solution. Subsequently, the two solutions were mixed rapidly, stirred for 30 min, and set aside at room temperature for 24 h. After centrifuging, washing with deionized water and ethanol several times, and drying in an oven at 60 °C for 6 h, a white precipitate was harvested. The precipitates were then transferred to a tube furnace and annealed in air at 600 °C for 2 h to form final products.

2.2. Materials characterization

The synthesized products were characterized by powder X-ray diffraction (XRD, Rigaku-D/Max 2500PC/Japan, using Cu Kα radiation, $\lambda = 1.5406$ Å), field emission scanning electron microscopy (FESEM, FEIXL-30/USA), and transmission electron microscopy (TEM, FEI-TECNAI G2 F20/America, operating at an accelerating voltage of 200 kV). Brunauer–Emmett–Teller (BET) surface area and pore volume were estimated using ASAP 2420 (USA).

2.3. Electrochemical measurements

The products were mixed with acetylene black and polyvinylidene fluoride which was resolved in *N*-methyl-2-pyrrolidone at a weight ratio of 80:10:10. The slurry was uniformly pasted on Al foil. Such prepared electrode sheets were dried at 120 °C for 12 h in a vacuum oven. The CR2025-type half-coin cells were assembled in an argon-filled glove box with H_2O and O_2 contents below 1 ppm. Metallic lithium foil was used as the counter and reference electrode. The electrolyte consists of a solution of 1 M $LiPF_6$ in mixture of ethylene carbonate (EC), ethyl methyl carbonate (EMC) and dimethyl carbonate (DMC) with a EC: EMC: DMC volume ratio of 1:1:1. Charge–discharge performance was evaluated by a LAND CT2001A battery instrument at a constant current density in the voltage range of 0.8–2.5 V at room temperature. Cyclic voltammetry measurements were carried out on a CHI650D electrochemical workstation over the potential range 0.8–2.5 V vs. Li/Li^+ at a scanning rate of 0.1 mVs^{-1}.

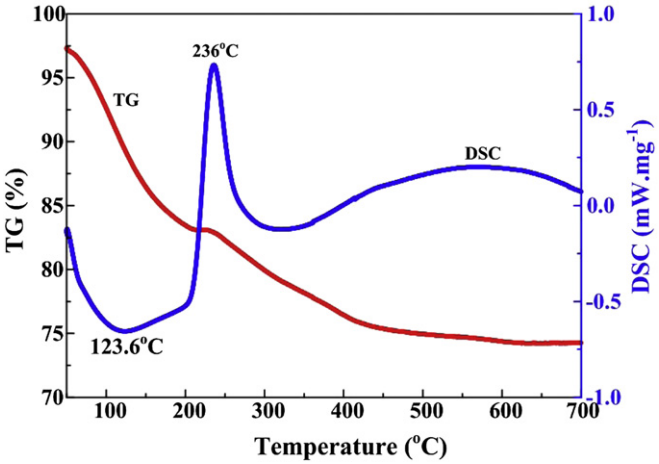

Fig. 1. TG-DSC curves of precursor.

3. Results and discussion

The TG-DSC curves of precursor powders are obtained with a heating rate of 10 °C min^{-1} from 50 to 700 °C and show in Fig. 1. Three distinct steps of weight loss are observed during heating process. The first step of weight loss, observed between 50 and 212 °C, is mainly due to the quick dehydration, which corresponds to an endothermic peak around 123.6 °C on TG-DSC curves. At the second step (212–500 °C), one obvious exothermic transformation at 236 °C is observed from the DSC graph, which is attributed to the combustion of residue surfactant as well as release of CO_2 and gases. At the same time, this process is accompanied with a huge weight loss. At the third step above 500 °C, no weight loss and no obvious thermal effect are observed, except that a slow exothermic process seems to occur. This slight exothermic process might be due to the crystallization of $Li_4Ti_5O_{12}$ [20,31].

Structure of as-synthesized precursors and calcined products at 600 °C for 2 h are inspected by X-ray diffraction (XRD) and shown in Fig. 2. No significant peaks are detected before calcination (Fig. 2(a)), revealing precursors being amorphous phases. After calcination, however, it converts to spinel lithium titanate (cubic phase) in accordance with spinel $Li_4Ti_5O_{12}$ (JCPDS Card No. 49-0207). The lattice parameter obtained by analyzing XRD pattern is estimated to be 8.365 Å, consistent with the report in previous reference [8].

Fig. 3(a) displays typical field emission scanning electron microscopy (FESEM) image of products after calcination. Interestingly, the $Li_4Ti_5O_{12}$ prepared here exhibits nearly spherical

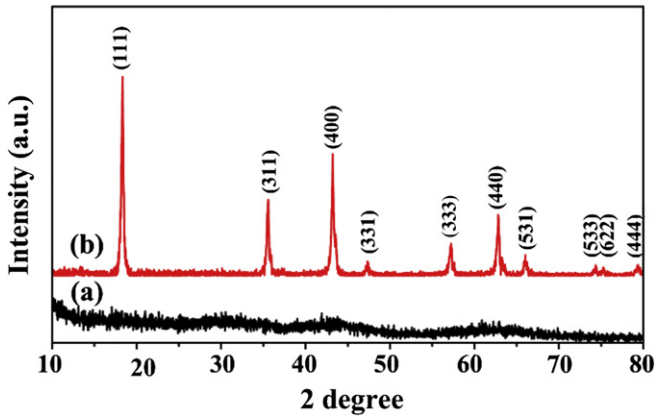

Fig. 2. XRD patterns of (a) precursor and (b) after calcination at 600 °C.

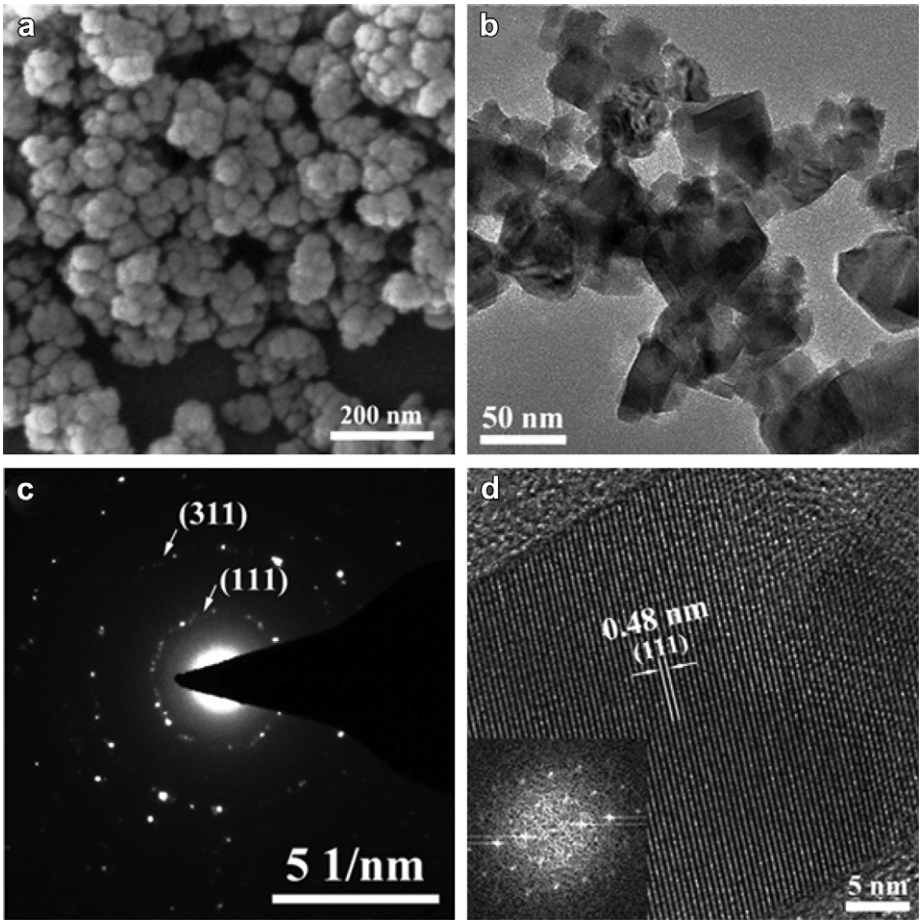

Fig. 3. Morphology and SAED of nanocryctalline $Li_4Ti_5O_{12}$: (a) Field emission scanning electron microscopy (FESEM) image, (b) Transmission electron microscopy (TEM) image, (c) Selected area electron diffraction (SAED) pattern, (d) High resolution TEM image (in set the corresponding fast Fourier transform pattern (FFT)).

aggregated morphology. Seemingly, the aggregates are composed of nanoparticles. To explore inherent structures, the aggregates are dispersed in the ethanol with sonication for 1 h and further characterized by TEM, as shown in Fig. 3(b). Clearly, the $Li_4Ti_5O_{12}$ achieved here displays a cubic morphology with sizes ranging around ~30–50 nm. The selected area electron diffraction (SAED) pattern is shown in Fig. 3(c). It displays strong ring patterns due to (111) and (311) planes, which coincides with spinel $Li_4Ti_5O_{12}$. The high-resolution TEM (HRTEM) image of $Li_4Ti_5O_{12}$ reveals a high crystallinity (Fig. 3(d)), and the interplanar distance is calculated to be ca. 0.48 nm, corresponding to the d-spacing of the (111) crystal plane. The highly crystallized spinel phase can greatly improve the crystallographic-structure stability and charge–discharge cycling ability of the $Li_4Ti_5O_{12}$ anode [24,32]. In addition, the corresponding Fast Fourier transform (FFT) pattern confirms the single crystal (inset of 3(d)).

Fig. 4 shows the N_2 adsorption/desorption isotherms and the Barrett–Joyner–Halenda (BJH) pore-size distribution curve (inset) of nanocrystalline $Li_4Ti_5O_{12}$. The N_2 adsorption/desorption isotherms are identified as the type IV (IUPAC classification), which is characteristic of mesoporous materials [22,33]. The pore-size distribution possesses a narrow peak and a broad peak centered at 2.5 and 30 nm in the sample, respectively. The Brunauer–Emmett–Teller (BET) specific surface area of the sample is 46.3 m^2g^{-1}.

Fig. 5 represents cyclic voltammogram of the nanocrystalline $Li_4Ti_5O_{12}$ electrode at a scan rate of 0.1 mVs^{-1}, after the first cycle at 0.2 C. One pair of peaks corresponds to the process of insertion and extraction of Li ions. A cathodic peak located at 1.52 V corresponds to the voltage plateau of the discharge process, which is the process of Li^+ insertion into nanocrystalline $Li_4Ti_5O_{12}$. Another anodic peak located at 1.65 V corresponds to voltage plateau of the charge process, indicating the process of Li^+ deintercalation from nanocrystalline $Li_4Ti_5O_{12}$ [14,34,35]. The potential difference between

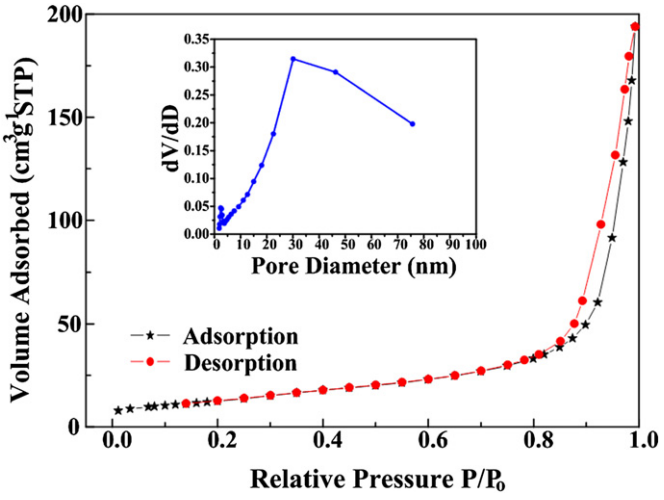

Fig. 4. Nitrogen adsorption–desorption isotherms of nanocrystalline $Li_4Ti_5O_{12}$ (inset graph: corresponding Barrett–Joyner–Halenda (BJH) distribution).

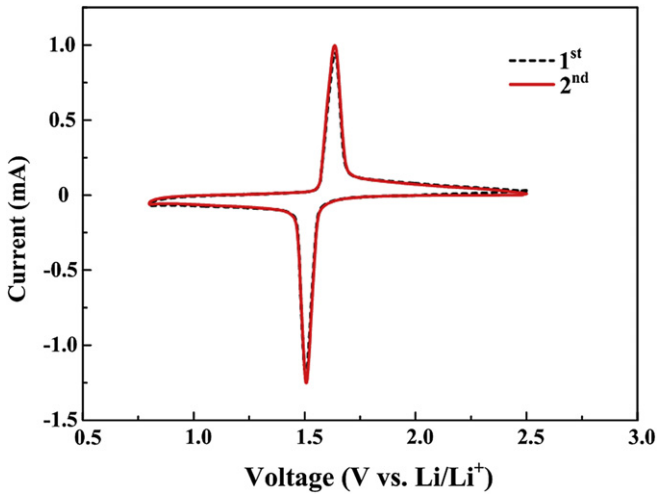

Fig. 5. Cyclic voltammograms (CV) of nanocrystalline $Li_4Ti_5O_{12}$ at scan rate of 0.1 mVs^{-1}.

anodic and cathodic potentials peak is about 0.13 V, which is larger than previous results obtained by some authors [36,37], but smaller than the result obtained by other authors [19,38]. The difference is mainly attributed to the lithium ion diffusivity rate verifying in various spinels $Li_4Ti_5O_{12}$ with different morphology and microstructure.

The electrochemical performance of the nanocrystalline $Li_4Ti_5O_{12}$ as anode materials for lithium-ion batteries has been investigated. Fig. 6(a) shows the first discharge–charge curves of nanocrystalline $Li_4Ti_5O_{12}$ at different current density between the voltage limits of 0.8 and 2.5 V. In agreement with the above CV analysis, two distinct voltage plateaus can be observed during the discharge–charge process. The cell flat voltage decreases with an increase in current density. It is 1.52 V at 0.2 C and drops to 1.45 V at 10 C. In addition, the discharge capacity exhibits a tendency to decrease on the increase of the discharge–charge current density, probably due to the low electronic conductivity of $Li_4Ti_5O_{12}$. The initial discharge capacity is 218, 202 and 162 $mAhg^{-1}$ at 0.2, 1 and 5 C, respectively. Among them at 0.2 and 1 C, its first discharge capacity slightly surpassed the theoretical value of pure $Li_4Ti_5O_{12}$ (175 $mAhg^{-1}$). Similar phenomena have been observed in previous literature [14,21,22,39]. Tang et al. [21] synthesized flower-like spinel $Li_4Ti_5O_{12}$ by hydrothermal process, and the first discharge capacity is 217.6 $mAhg^{-1}$ at 0.2 C. The extra discharge capacity may be explained by some titanium possibly present in the form of TiO_2 in the product, despite that its diffraction peak is not detected by XRD, which has a theoretical capacity exceeding that of $Li_4Ti_5O_{12}$. At the very high rate of 10 C, the specific discharge capacity is still 163 $mAhg^{-1}$, while those with anodes consisting of bulk $Li_4Ti_5O_{12}$ discharge only to 30–60% at the same discharge current density [40,41]. Moreover, the nanocrystalline $Li_4Ti_5O_{12}$ also exhibits an excellent cyclability at different current densities and is shown in Fig. 6(b). After the initial capacity loss, all these samples display very high capacity retention upon cycling. After 50 discharge/charge cycles, specific capacities still remain in 174 and 166 $mAhg^{-1}$ at 0.2 and 1 C, respectively. The fading of the total capacities is 7.4 and 4.8% at 0.2 and 1 C during the 2–50th cycles, respectively. When the current rate increases to 5 C, a capacity of 136 $mAhg^{-1}$ can still be delivered. It is quite interesting to discover that a further increase in the current rate to 10 C leads only to an insignificant drop in capacity to 130 $mAhg^{-1}$ after 50 cycles. Note that the excellent electrochemical performance achieved in this study is slightly higher than some results reported recently [13,42,43]. Lee

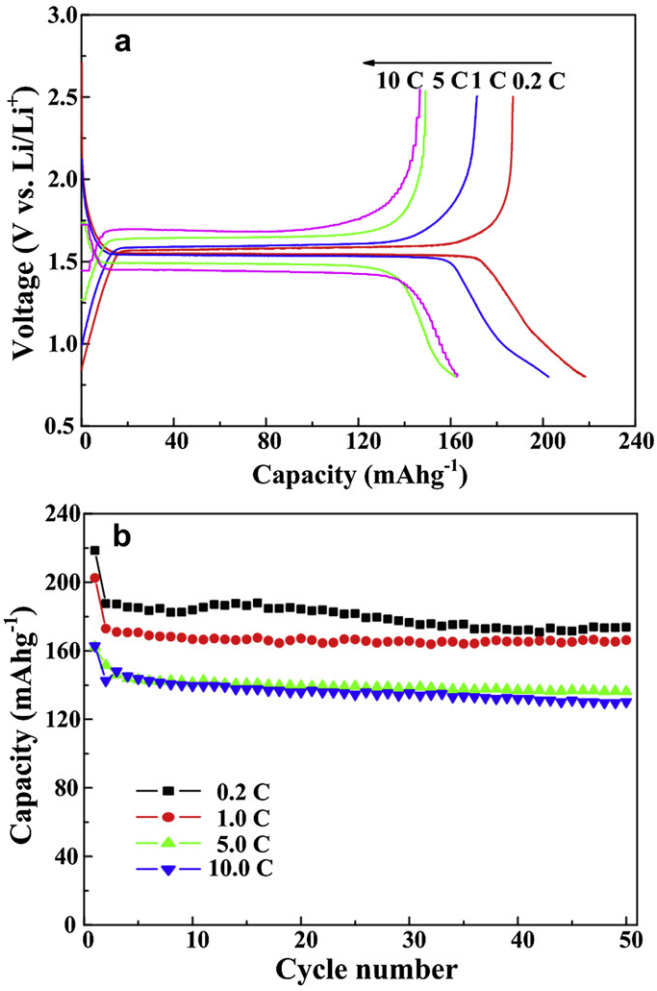

Fig. 6. Electrochemical measurements of nanocrystalline $Li_4Ti_5O_{12}$: (a) The first charge–discharge voltage profiles at different current densities, (b) Cycling performance at different current densities.

et al. [13] synthesized spinel $Li_4Ti_5O_{12}$ nanotube via heat treatment and alkali–hydrothermal reactions, and the reversible capacity was approximately 156 $mAhg^{-1}$ at a current rate of 0.1 C. Yin et al. [42] synthesized $Li_4Ti_5O_{12}$ particle (about 140 nm) by a modified rheological phase method, and the anode exhibited discharge capacities of 161.6 and 112.3 $mAhg^{-1}$ after 50 cycles at current rates of 1 and 10 C, respectively. Deng et al. [43] prepared $Li_4Ti_5O_{12}$ thin film by pulsed laser deposition technique and annealed at 700 °C, and the steady-state discharge capacity was about 157 $mAhg^{-1}$ at a current density of 0.58 C. Presumably, the good electrochemical performance can be attributed to i) the nano-size of particles increasing effective interfacial reactivity and shortening diffusion distances of intercalated lithium ions, and ii) the high degree of crystallization keeping the structure integrity during the Li^+ intercalation/deintercalation process and accelerating the lithium ions and electrons diffusion in solid bulk phase [24]. Besides, the presence of abundant mesopores or macropores among aggregates allows electrolyte to easily infiltrate into the pores to contact the embedded nanocrystalline $Li_4Ti_5O_{12}$ [10].

4. Conclusions

In this study, we have demonstrated a facile and simple synthetic route for preparing nanocrystalline $Li_4Ti_5O_{12}$. As-

prepared $Li_4Ti_5O_{12}$ nanocrystalline measures around 30–50 nm and has high crystallinity. As anode materials, $Li_4Ti_5O_{12}$ nanocrystalline prepared here exhibits high discharge capacity of 218.4 $mAhg^{-1}$ at 0.2 C in the first cycle and favorable cycling stability at high current density such as 5 and 10 C. The ultrahigh rate capability and good cycling performance might be attributed to the merit of nanosized particles, high crystallinity, and abundant mesopores and macropores. Therefore, the nanocrystalline $Li_4Ti_5O_{12}$ is promising for such extensive applications as anode material for high-power Li-ion batteries.

Acknowledgement

This work is supported by Foundation of Jilin University for Distinguished Young Scholars. Partial financial support comes from Project 985-High Performance Materials and Advanced Manufacturing Technology of Jilin University.

References

[1] M. Armand, J.M. Tarascon, Nature 451 (2008) 652–657.
[2] Y. Idota, T. Kubota, A. Matsufuji, Y. Maekawa, T. Miyasaka, Science 276 (1997) 1395–1397.
[3] H.G. Jung, M.W. Jang, J. Hasspun, Y.K. Sun, B. Scrosati, Nat. Commun. (2011). http://dx.doi.org/10.1038/ncomms1527.
[4] J.M. Tarascon, M. Armand, Nature 414 (2001) 359–367.
[5] J.B. Goodenough, Y. Kim, Chem. Mater. 22 (2009) 587–603.
[6] E.P. Roth, D.H. Doughty, J. Franklin, J. Power Sources 134 (2003) 224–227.
[7] J.S. Kim, S.W. Kim, H. Gwon, W.S. Yoon, K. Kang, Electrochim. Acta 54 (2009) 5914–5918.
[8] T. Ohzuku, A. Ueda, N. Yamamoto, J. Electrochem. Soc. 142 (1995) 1431–1435.
[9] E.M. Sorensen, S.J. Barry, H.K. Jung, J.R. Rondinelli, J.T. Vaughey, K.R. Poeppelmeier, Chem. Mater. 18 (2006) 482–489.
[10] L.F. Shen, C.Z. Yuan, H.J. Luo, X.G. Zhang, K. Xu, F. Zhang, J. Mater. Chem. 21 (2011) 761–767.
[11] L. Cheng, J. Yan, G.N. Zhu, J.Y. Luo, C.X. Wang, Y.Y. Xia, J. Mater. Chem. 20 (2010) 595–601.
[12] G.J. Wang, J. Gao, L.J. Fu, N.H. Zhao, Y.P. Wu, T. Takamura, J. Power Sources 174 (2007) 1109–1112.
[13] S.C. Lee, S.M. Lee, J.W. Lee, J.B. Lee, S.M. Lee, S.S. Han, H.C. Lee, H.J. Kim, J. Phys. Chem. C 113 (2009) 18420–18423.
[14] J.Z. Chen, L. Yang, S.H. Fang, Y.F. Tang, Electrochim. Acta 55 (2010) 6596–6600.
[15] B.B. Tian, H.F. Xiang, L. Zhang, Z. Li, H.H. Wang, Electrochim. Acta 55 (2010) 5453–5458.
[16] J. Wolfenstine, J.L. Allen, J. Power Sources 180 (2008) 582–585.
[17] H.G. Jung, S.T. Myung, C.S. Yoon, S.B. Son, K.H. Oh, K. Amine, B. Scrosati, Y.K. Sun, Energy Environ. Sci. 4 (2011) 1345–1351.
[18] M.M. Rahman, J.Z. Wang, M.F. Hassan, S.L. Chou, D. Wexler, H.K. Liu, J. Power Sources 195 (2010) 4297–4303.
[19] J.R. Li, Z.L. Tang, Z.T. Zhang, Electrochem. Commun. 7 (2005) 894–899.
[20] D. Wang, N. Ding, X.H. Song, C.H. Chen, J. Mater. Sci. 44 (2009) 198–203.
[21] Y.F. Tang, L. Yang, Z. Qiu, J.S. Huang, Electrochem. Commun. 10 (2008) 1513–1516.
[22] Y. Tang, L. Yang, S. Fang, Z. Qiu, Electrochim. Acta 54 (2009) 6244–6249.
[23] M.R. Jo, K.M. Nam, Y.M. Lee, K. Song, J.T. Park, Y.M. Kang, Chem. Commun. 47 (2011) 11474–11476.
[24] N.Q. Zhang, Z.M. Liu, T.Y. Yang, C.L. Liao, Z.J. Wang, K.N. Sun, Electrochem. Commun. 13 (2011) 654–656.
[25] A.S. Prakash, P. Manikandan, K. Ramesha, M. Sathiya, J.M. Tarascon, A.K. Shukla, Chem. Mater. 22 (2010) 2857–2863.
[26] J.H. Schulman, W. Stoeckenims, L.M. Princ, J. Phys. Chem. 63 (1959) 1677–1680.
[27] M.J. Schwuger, K. Stickdornt, Chem. Rev. 95 (1995) 849–864.
[28] H. Groger, F. Gyger, P. Leidinger, C. Zummuhl, C. Feldmann, Adv. Mater. 21 (2009) 1586–1590.
[29] A.K. Ganguli, T. Ahmad, S. Vaidya, J. Ahmed, Pure Appl. Chem. 80 (2008) 2451–2477.
[30] V. Juttukonda, R.L. Paddock, J.E. Raymond, D. Denomme, A.E. Richardson, L.E. Slusher, B.D. Fahlman, J. Am. Chem. Soc. 128 (2006) 420–421.
[31] Y.J. Hao, Q.Y. Lai, J.Z. Lu, H.L. Wang, Y.D. Chen, X.Y. Ji, J. Power Sources 158 (2006) 1358–1364.
[32] J.C. Arrebola, A. Caballero, M. Cruz, L. Hrenan, J. Morales, E.R. Castellon, Adv. Funct. Mater. 16 (2006) 1904–1912.
[33] A. Vinu, D.P. Sawant, K. Ariga, M. Hartmann, S.B. Halligudi, Microporous Mesoporous Mater. 80 (2005) 195–203.
[34] C. Lai, Y.Y. Dou, X. Li, X.P. Gao, J. Power Sources 195 (2010) 3676–3679.
[35] L. Shen, C. Yuan, H. Luo, X. Zhang, K. Xu, Y. Xia, J. Mater. Chem. 20 (2010) 6998–7004.
[36] H.W. Lu, W. Zeng, Y.S. Li, Z.W. Fu, J. Power Sources 164 (2007) 874–879.
[37] S. Bach, J.P. Pereira-Ramos, N. Baffier, J. Power Sources 81/82 (1999) 273–276.
[38] J. Li, Y.L. Jin, X.G. Zhang, H. Yang, Solid State Ionics 178 (2007) 1590–1594.
[39] Z. Wang, R. Cai, S. Jiang, Z. Shao, J. Mater. Chem. (2012). http://dx.doi.org/10.1039/c2jm33346e.
[40] S.H. Huang, Z.Y. Wen, J.C. Zhang, X.L. Yang, Electrochim. Acta 52 (2007) 3704–3708.
[41] H. Kitaura, A. Hayashi, K. Tadanaga, M. Tatsumisago, J. Power Sources 189 (2009) 145–148.
[42] S.Y. Yin, L. Song, X.Y. Wang, M.F. Zhang, K.L. Zhang, Y.X. Zhang, Electrochim. Acta 54 (2009) 5629–5633.
[43] J. Deng, Z. Lu, I. Belharouak, K. Amine, C.Y. Chung, J. Power Sources 193 (2009) 816–821.